



Autonomous fault detection and diagnosis for permanent magnet synchronous motors using combined variational mode decomposition, the Hilbert-Huang transform, and a convolutional neural network

Ma'd El-Dalahmeh^a, Maher Al-Greer^{a,*}, Imran Bashir^a, Mo'ath El-Dalahmeh^a, Aykut Demirel^b, Ozan Keysan^b

^a School of Computing, Engineering and Digital Technologies, Teesside University, Middlesbrough, UK

^b School of Engineering, Middle East Technical University, Ankara, Turkey



ARTICLE INFO

Keywords:

Fault detections
Condition monitoring
Electrical machines
Permanent magnet synchronous motor
Convolution neural network
Variational mode decomposition
Hilbert-Huang transform

ABSTRACT

The continuous and online monitoring of the condition of electrical machines is key to their safe operation. This study introduces a novel fault detection and diagnosis technique for continuous monitoring of faults in permanent magnet synchronous motors (PMSM). The proposed method relies solely on built-in sensors (stator phase currents only) to detect three types of faults: inter-turn short circuit, partial demagnetisation, and static eccentricity. Our fault detection and diagnosis strategy was developed by combining variational mode decomposition (VMD), the Hilbert-Huang transform (HHT) and a convolutional neural network (CNN). The VMD is first applied to the stator phase current signals to analyse the characteristic behaviour of the current signals by decomposing the current signals into several intrinsic mode functions. The intrinsic mode functions of the healthy and faulty signals are compared, and that with the frequency shift characteristics is selected. HHT is then applied to extract the fault feature by calculating the instantaneous frequency. Finally, the instantaneous frequency feature is fed into the CNN, which is designed to detect and classify motor faults. Experimental results clearly show that the variation of the instantaneous frequency of the PMSM, working at different operating states, can be utilised for condition monitoring and fault detection.

1. Introduction

Recently, PMSMs have seen a substantial growth in usage for various applications, including wind turbines, electric vehicles, electrical traction, and others. The PMSM is preferred because of its high-performance characteristics, which include efficiency, power density, and torque [1]. Moreover, PMSMs have been used for a long time, usually under challenging and demanding work circumstances with high heat cycles. These conditions can, however, result in various PMSM faults, and so monitoring and early detection are critical for preventing system failure to reduce significant downtime and lower maintenance costs. High reliability and safety levels are necessary for critical missions and high-cost applications [2]. Therefore, numerous condition monitoring (CM) and fault detection (FD)

* Corresponding author.

E-mail address: M.Al-Greer@tees.ac.uk (M. Al-Greer).

methods have been reported in the literature. Generally, these methods can be categorised into model-based methods and data-driven methods [1].

Model-based fault detection methods work by building a model based on physical theories that include a specific fault, and then comparing the model's estimated output to the detected true output to validate whether the fault happened in the motor. A range of model-based methodologies have been developed, including mathematical, magnetic equivalent circuit (MEC), and finite element models (FEM) [3]. These techniques have proven highly reliable and accurate in detecting faults in motors. The authors of [3] compared the performance of these model-based strategies. Although model-based approaches have some advantages, they also face numerous difficulties, such as the computational complexity of FEM and the accuracy constraints of mathematical and MEC models. They also require particular motor and drive system parameters to generate consistent results [4]. Even when the parameters are accurate, this method may be unsuitable for low-cost motor drivers due to their computational load. For example, the authors of [5] developed a simplified physical faulty model of PMSM to diagnose the inter-turn short circuit fault (ITSC), phase-to-phase faults, and phase-to-ground faults. While their approach proved to be successful in diagnosing faults, it was found to be computationally demanding and necessitated extensive training prior to detecting any faults.

Unlike model-based approaches, data-driven methods have recently attracted greater attention due to their clarity and being model-free. In data-driven methodology, CM/FD systems must learn the underlying functional relationships between the measured signals and component faults in order for the latter to be detected and classified. Artificial intelligence (AI)/machine learning (ML) algorithms are used to build such functional relationships. For example, in [6], a recurrent neural network (RNN) model was applied to detect the ITSC fault in PMSMs. The RNN was fed the three-phase currents and rotating speed as input features for both training and fault diagnosis purposes. In [7], a wavelet convolutional neural network (WCNN) was proposed for an open circuit fault diagnosis in PMSMs. The authors of [8] proposed an ITSC and misalignment faults diagnosis method which is based on transforming the measured stator current signals of the PMSM into 2-D images, using an instantaneous current residual map (ICRM). The converted images are then fed into a CNN model for extraction of the fault diagnostic features.

It is worth noting that the accuracy of the FD/CM depends on the relevance of the diagnostic feature being extracted. Consequently, it is essential to obtain informative and diagnostic features from the observed signals when employing data-driven approaches. Studies have used various signal-processing techniques to extract the relevant features from the measured signals. Typical signal-processing techniques for extracting diagnostic features include domain analyses such as for time [9], frequency [10], and time-frequency [11], which are commonly used as signal-processing methodologies. For instance, in [9], 13 time-domain features were extracted to detect the broken rotor of a PMSM using the stator current signal under various load conditions. The extracted features are then used for fault detection using a random forest (RF) model.

In contrast, the authors of [10] detected and diagnosed the ITSC fault of PMSMs using spectral analysis of the negative and positive components of the stator currents. However, relying solely on features extracted from the time or frequency domains is ineffective. Specifically, employing the retrieved features from a single domain means that certain crucial features could be missed, potentially lowering the accuracy of the FD/CM. The collected signal is also typically nonstationary in an industrial field due to numerous sources of signal interference. In other words, signal frequency varies with time, and the frequency components present at each instant are distinct; hence, the signal lacks periodicity [16].

For the fault detection and diagnosis of nonstationary stator current signals, several time-frequency analysis methods have been applied, including wavelet transform (WT) [11], and short-time Fourier transform (STFT) [12]. For instance, the authors of [11] used a WT approach to detect ITSC faults in the stator windings of PMSMs. Specifically, the authors applied the WT to the cost function to extract the fault feature. The fault diagnosis was then achieved by monitoring the energy feature vector calculated from the WT coefficients. The authors in [12] detected the ITSC fault of the PMSM by applying the STFT to the stator current signal. Nevertheless, the basic idea in STFT analysis is the frequency indicating the signal's periodicity, which necessitates the signal's stationarity. Lack of periodicity is a feature of nonstationary signals. If the frequency is specified using Fourier analysis, spectrum analysis of nonstationary signals will lack a physical foundation [13]. Moreover, WT is not adaptive and is unsuitable for nonstationary signals as the mother wavelet is defined without any input from data.

The abovementioned techniques are not well-suited for nonstationary signals with varying frequencies over time. To address this, a new concept called instantaneous frequency (IF) has been introduced [14], which involves decomposing nonstationary signals into a set of signals that meet narrow-band requirements. This method only applies to single-component signals, but most signals in engineering are multicomponent signals. To tackle this issue, the empirical mode decomposition (EMD) method was proposed. The authors of [15] extracted the IF of the induction motor (IM) based on the EMD technique and adaptive IF estimation algorithm for ITSC fault detection. Moreover, the author of [16] detected demagnetisation faults in PMSMs by applying the EMD and Hilbert-Huang transform (EMD-HHT) methods to monitor the variation of the extracted instantaneous frequency feature.

However, the EMD depends solely on detecting local minima/maxima and estimates lower/upper envelopes by interpolation, which affects the reliability of fault diagnoses due to the lack of a mathematical basis and methods for interpolating and detecting local minima/maxima. The VMD method has demonstrated efficacy in fault diagnosis in a variety of applications, including FD in distribution networks [17] and wind turbine generators [18], amongst others. According to [22,23], VMD can resolve the problem of 'mode aliasing' by defining each mode as limited bandwidth. VMD solves the issues faced in EMD, such as mode mixing and the lack of a mathematical foundation. VMD is also a very robust technique for signal decomposition, and the signal can be reconstructed with a high degree of accuracy. Therefore, in [19], the VMD method was applied for ITSC and demagnetisation fault detection in PMSMs. More specifically, the stator current signal is decomposed by VMD, and the energy value of the intrinsic mode function (IMF) is used as the input feature for a fuzzy C-means clustering probabilistic neural network (FCM-PNN). The developed model achieved accuracy of up to 95%. Similarly, the VMD method was used for IM fault detection in [20].

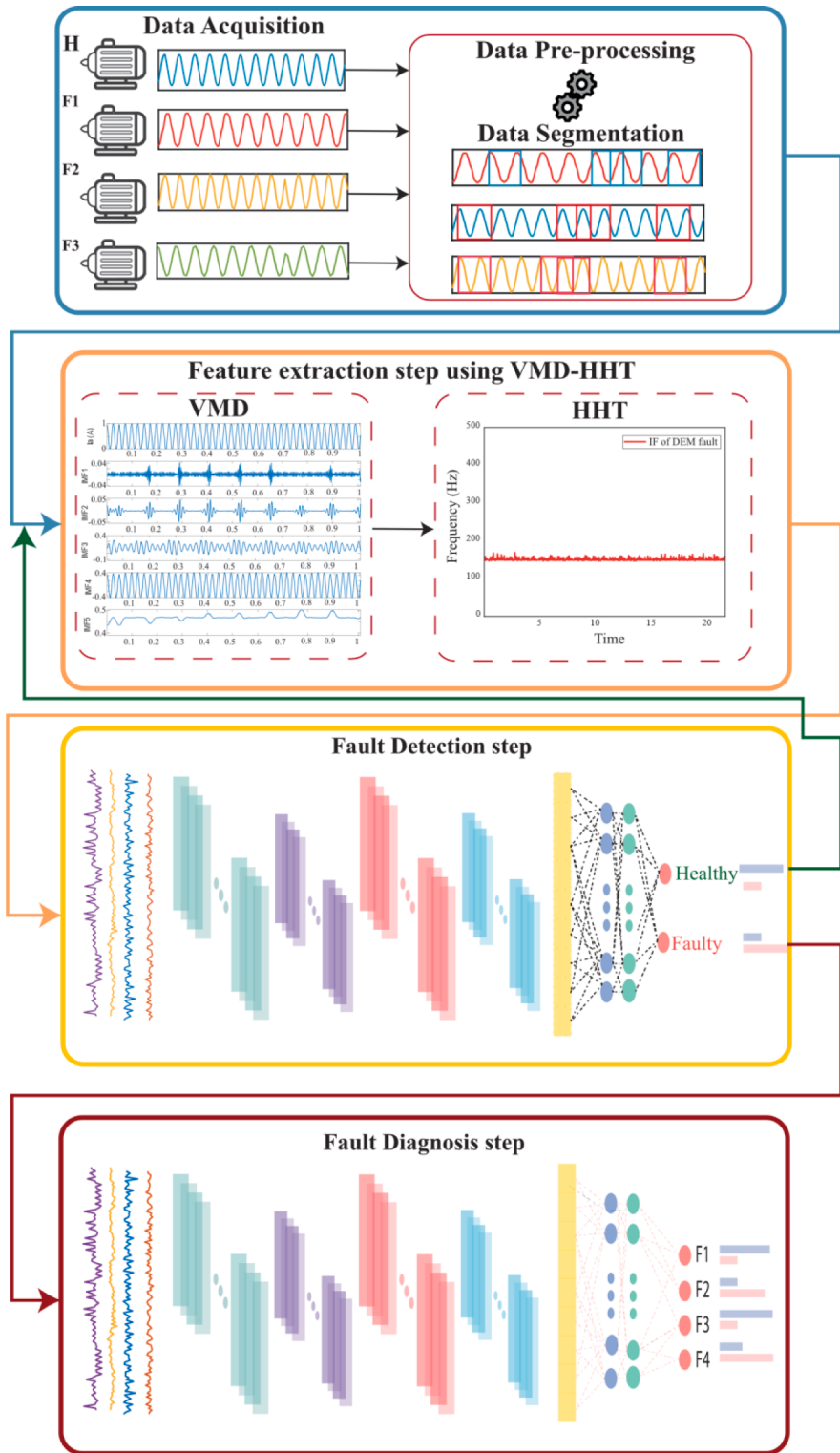


Fig. 1. The proposed method for fault detection and diagnosis in the PMSM.

In summary, in the literature, most of the proposed techniques focus on detecting one or two types of faults in the PMSM. Most also determine extracted features at fixed speed/load operating conditions and few studies have validated their approaches under varied working conditions. Lastly, most of the proposed methods are only tasked with fault detection, while a few focus on developing fault diagnoses and detection algorithms for PMSM. Therefore, in this paper, we propose an autonomous fault detection and diagnosis

method using VMD decomposition, IMF selection, HHT feature extraction by calculating the IF, and automated fault detection and diagnosis using two CNN models. The most common failures on PMSMs, such as stator ITSC fault, non-uniform demagnetisation of permanent magnets, and static rotor eccentricities, are detected and classified. To the author's knowledge, no previous work has devised a generic data-driven system to detect and classify these faults in PMSMs. In this study, we used the highly adaptive VMD time-frequency technique without adding much computational complexity compared to other time-frequency techniques. Our contributions can be summarised as follows:

- Development and investigation of the VDM-HHT method in PMSM fault detection and diagnosis for three types of faults (electrical and machinal faults), as well as predictive maintenance for reliable and safe operation;
- Extraction of the IF feature from the time and frequency domain to improve prediction accuracy;
- Requirement for no additional sensors because diagnostic features are extracted from the accessible stator current signals. The experimental results showed that the proposed technique accurately detects and classifies the faults, with a detection accuracy of 98.8%;
- Utilisation of existing data for continuous monitoring of the electrical machines by extracting the features using a combination of VMD, HHT and CNN.

The remainder of this paper is set out as follows: [Section 2](#) presents the mathematical depth theory of the proposed system and the methods for condition monitoring and fault detection; [Section 3](#) describes the experimental setup and data collection used in the developed algorithm; the results and discussion are presented in [Section 4](#); and the conclusions of this work are given in [Section 5](#).

2. Mathematical background and methods

The proposed method is divided into four main steps: data pre-processing, feature extraction based on VMD-HHT, and fault detection and then diagnosis using CNN models, as shown in [Fig. 1](#). The measured phase currents are collected from the experimental setup in the pre-processing data section. The obtained currents are then decomposed into several IMFs using the VMD process. Then, the most important IMF with an apparent fault signature is selected for the feature extraction process. Afterwards, the selected IMF is used for feature extraction IF by applying the HHT method. Finally, the extracted features based on the VMD-HHT approach are used to train two CNN models for fault detection and diagnosis. The following subsections describe the operating flow of the proposed detection and diagnosis methodology.

2.1. VMD-HHT based feature extraction

In this work, the stator phase current signals of the PMSM are analysed using VMD in conjunction with CNN to detect the three types of faults in the PMSM: ITSCF, non-uniform DEF, and SEF. Consider the measured stator three-phase current (I), written as:

$$I = I_a e^{j0} + I_b e^{j2\pi/3} + I_c e^{j4\pi/3} \quad (1)$$

Intrinsic mode functions take the shape of amplitude and frequency-modulated signals, which can be written as:

$$u(t) = A(t)\cos(\phi(t)) \quad (2)$$

Where, $A(t) \geq 0$ is a time-varying amplitude due to amplitude modulation and $\phi(t)$ time-varying phase due to frequency modulation with its derivative greater than zero.

The VMD is calculated in three steps; firstly, the analytic function is calculated using Hilbert transform. The analytic form $u(t)$ is obtained by taking its Hilbert transform, and a complex-unique analytic signal is defined as:

$$u_I(t) = u(t) + j\mathcal{H}(u(t)) = A(t)e^{j\phi(t)} \quad (3)$$

Where, the Hilbert transform is calculated as:

$$\mathcal{H}(u(t)) = \frac{1}{\pi} \int_{-\infty}^{\infty} \frac{u(t')}{t - t'} dt' \quad (4)$$

In the case of slow varying amplitude for IMF, the analytic signal inherits the same amplitude and is written as:

$$u_{k,A}(t) = A_k(t)e^{j\phi(t)} \quad (5)$$

The second step of VMD is to demodulate each frequency mode spectrum to a lower frequency through multiplication with complex exponential of the estimated centre frequency ω_k . The third step takes the resultant signal's derivative and squared L2-norm, respectively. Following all these steps, the constrained variational optimisation problem can be described as:

$$\text{minimize } (u_k), (\omega_k) \left\{ \sum_k \left\| \partial_t [u_k^k(t) e^{-i\omega_k t}] \right\|_2^2 \right\} \quad (6)$$

Where, u_l^k is the analytic signal, ∂_t is the partial derivative, and ω_k is the centre frequency. Eq. (6) gives the VMD, which decomposes the input signal $I(t)$ into a finite and predefined k number of intrinsic modes $u_k(t)$, which should be added to reconstruct the input signal.

$$\sum_k u_k(t) = I(t) \quad (7)$$

Now, the reconstruction constraint can be addressed by augmented Lagrangian [8]. There are two penalty terms, such as a quadratic term to enforce reconstruction fidelity and a term with Lagrangian multipliers λ to ensure that the constraints are strictly fulfilled. The resulting augmented Lagrangian function can be given as:

$$L((u_k), (\omega_k), \lambda) = \alpha \sum_k \partial_i \{ u_i^k(t) e^{-i\omega_k t} \}_2^2 + I(t) - \sum_k u_k(t)_2^2 + \lambda(t), I(t) - \sum_k u_k(t) \quad (8)$$

The solution of the Lagrangian function is obtained through optimisation. The minimisation problem given in (8) is solved in the spectral domain within VMD to calculate modes, as shown in (9).

$$\hat{u}_k^{n+1}(\omega) = \frac{\hat{I}(\omega) - \sum_{i \neq k} \hat{u}_i(\omega) + \frac{\lambda(\omega)}{2}}{1 + 2\alpha(\omega - \omega_k)^2} \quad (9)$$

This is clearly identified as a Wiener filtering of the current residual, with a signal prior $1/(\omega - \omega_k)^2$. The full spectrum of the real mode is then obtained by Hermitian symmetric completion. The centre frequency can be calculated by running the optimisation problem as presented in (10).

$$\omega_k^{n+1} = \frac{\int_0^\infty \omega |\hat{u}_k(\omega)|^2 d\omega}{\int_0^\infty |\hat{u}_k(\omega)|^2 d\omega} \quad (10)$$

This puts the new ω_k at the centre of gravity of the corresponding mode's power spectrum. Thus, carrier frequency is the frequency of a least square linear regression to the instantaneous phase observed in the mode. Once the input signal is decomposed into IMFs by VMD, the corresponding IF is calculated using HHT [21]. The amplitude and phase for the analytic signal given in (3) and (5) can be written as:

$$A(t) = \sqrt{(u(t))^2 + \left(\frac{1}{\pi} \int_{-\infty}^{\infty} \frac{u(i)}{t-t'} dt' \right)^2} \quad (11)$$

$$\phi(t) = \tan^{-1} \left(\frac{u(t)}{\frac{1}{\pi} \int_{-\infty}^{\infty} \frac{u(i)}{t-t'} dt'} \right) \quad (12)$$

The corresponding IF of the resultant IMFs decomposed by VMD is calculated by taking the derivative of the phase of HHT based analytic signal.

$$IF_k = \frac{d\phi(t)}{dt} \quad (13)$$

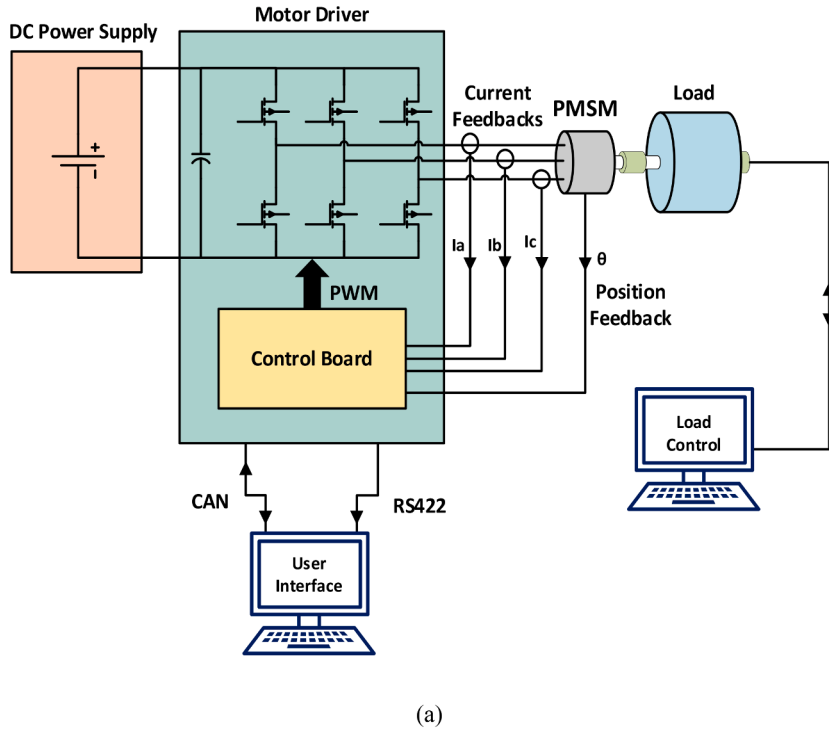
Where, IF_k is the instantaneous frequency calculated by taking the HHT transformation of the k th IMF component of phase current, k th is the number of IMF components, $k = 1, 2, 3, \dots, n$. The instantaneous output frequency is trained through a convolutional neural network (CNN) in order to develop a fully automated fault-detecting system.

2.2. CNN algorithm for fault detection and diagnosis

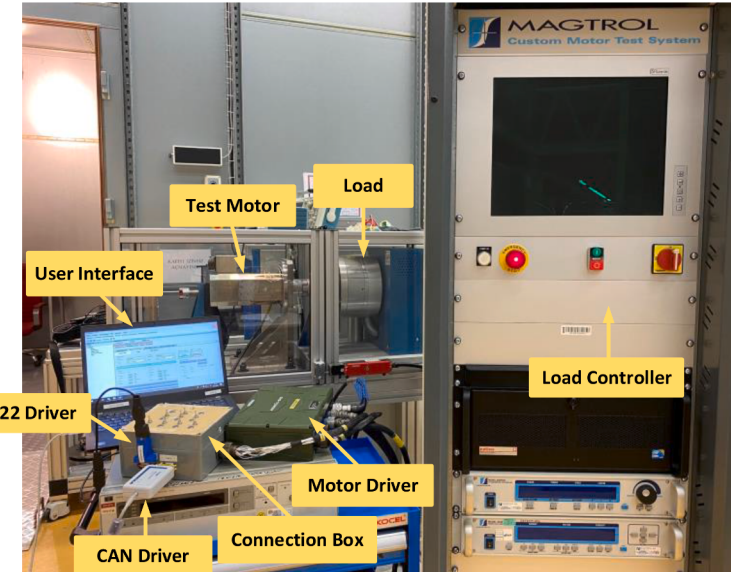
The fault features extracted by VMD-HHT for different fault conditions are fed as an input vector to the CNN predictive model to determine the association between extracted fault features and the classification of faults, as well as the identification of fault locations. The CNN algorithm is built on a mathematical basis that often mainly consists of three types of layers: convolution, pooling, and fully connected layers. The first two layers of convolution and pooling are linked to form a set of several convolution blocks piled on top to build a complex structure to perform the extracted features. The third, fully connected layer maps the data features extracted into the final output, such as classification [22].

The convolution layer is formed by the input data set of the initial layer and the filter kernels. Thus, a series of weights called filter banks connect each convolutional layer's units to local patches to create a features map. The convolution of the input maps yields the output features map, calculated as:

$$x_j^l = f \left(\sum_{i \in M_j} x_i^{l-1} * K_{ij}^l + b_j^l \right) \quad (14)$$



(a)



(b)

Fig. 2. (a) Schematic and (b) experimental setup.

Where, $*$ represents the conventional operation, x_i is i th input map, k denotes $F \times F$ matrix of a convolutional filter, M_j is the convolutional layer's feature map, b_j is the additive bias, and l is the number of layers in CNN algorithm. Finally, the outputs from the convolutional layers are input into the activation function. Rectified linear unit (ReLU) is the most often used activation function, defined as shown in (15).

$$\text{ReLU}(x) = \max(0, x) \quad (15)$$

For the pooling layer, low-resolution maps are constructed from the necessary local information to extract corrections. The max pooling layer is based on extracting maximum values from each patch and discarding all the lowest values. A fully connected layer uses

Table 1

Electrical and mechanical specification of the PMSM.

Property	Value
Winding	3-phase Y-connected
Rated voltage	18–32 V
Rated current	18.67 Arms
Rated torque	1.68 Nm
Rated speed	2300 rpm
Rated power	400 W
Number of pole pairs	4
Number of stator slots	27
Moment of inertia	0.374 kg.cm ²
Stator and rotor length	40 mm
Stator outer diameter	68 mm
Rotor outer diameter	33 mm
Air-gap length	1.8 mm
Motor driver	3-phase voltage source inverter
Control	Field-orientated control with space vector pulse width modulation (SVPWM)
Software	Embedded C code on TMS320C6713 Digital Signal Processor (DSP)

Table 2

Test conditions for the PMSM.

	0 Nm	0.4 Nm	0.8 Nm	1.2 Nm	1.6 Nm
600 rpm	✓	✓	✓	✓	✓
1200 rpm	✓	✓	✓	✓	✓
1800 rpm	✓	✓	✓	✓	✓
2400 rpm	✓	✓	✓	✓	✓

one-dimensional vectors to represent all feature maps in the output layer that are ultimately linked. The output of the fully connected layer is described in (16).

$$O_i = f \left(\sum_{j=1}^d x_i^f w_{ij} + b_j \right) \quad (16)$$

Where, O_i denotes the main output layer, x_i^f is the j^{th} neuron in the fully connected layer, w_{ij} represents the weight related to O_i and x_i^f , b_j is the bias corresponding to O_i , and f is the activation function [22].

The model's input layer is the instantaneous frequency vector extracted by VMD-HHT (3)–(13). The vector is defined as:

$$IF = \{f_1, f_2, f_3, \dots, f_k\} \quad (17)$$

Where, f_k represents the fault frequency feature vector extracted by HHT transforms and an IMF component of the stator current of the PMSM $k = 1, 2, 3, \dots, n$.

The fault feature vector (IF) is fed into the trained CNN fault diagnosis model to classify the fault type and determine its location. For fault classification, the SoftMax method [22] is used after the fully connected layer to judge the fault. The SoftMax output represents the probability that the sample is part of a particular class. Then, the location or type of fault is obtained by comparing the output probability of each fault type. SoftMax classifier's multi-class classification structure is as:

$$P(z_j) = \frac{e^{z_j}}{\sum_{i=1}^n e^{z_i}} \quad (18)$$

Where, $P(z_j)$ denotes the probability of output of the j^{th} neuron, n refers to the total number of fault categories, and a neuron's output is represented by z_j and z_i , respectively, in a fully connected layer.

3. Experimental setup, data collection and analysis

In this work, multiple testing was carried out to collect the experimental data of the PMSM and validate the proposed paradigm. The collected data for the PMSM is highly valuable as this data collection campaign is challenging to conduct in specific conditions and requires significant resources. The data were collected in a closed loop with the current control loop utilising a proportional-integral controller (PI), and speed control must be emphasised. Most previous research has relied on ideal conditions and open-loop setups to gather data that could be used for modelling and parameter estimation to detect faults, but studies have neglected to consider the impact of the actual closed-loop operation on accurate correlation of the extracted features with the faults; the influence of noise has also been ignored. To the best of our knowledge, no data sets are available which consider three different sorts of faults, possibly

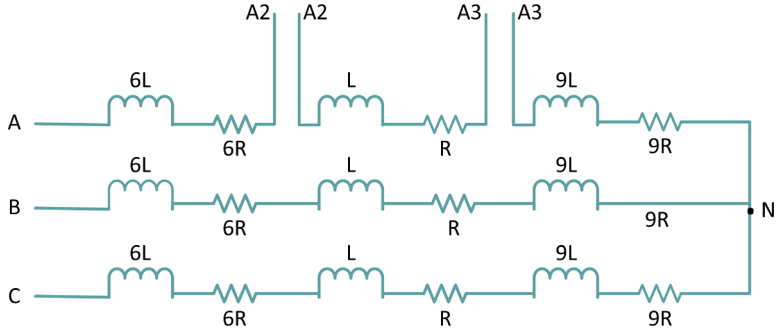


Fig. 3. Winding and terminals of the stator.

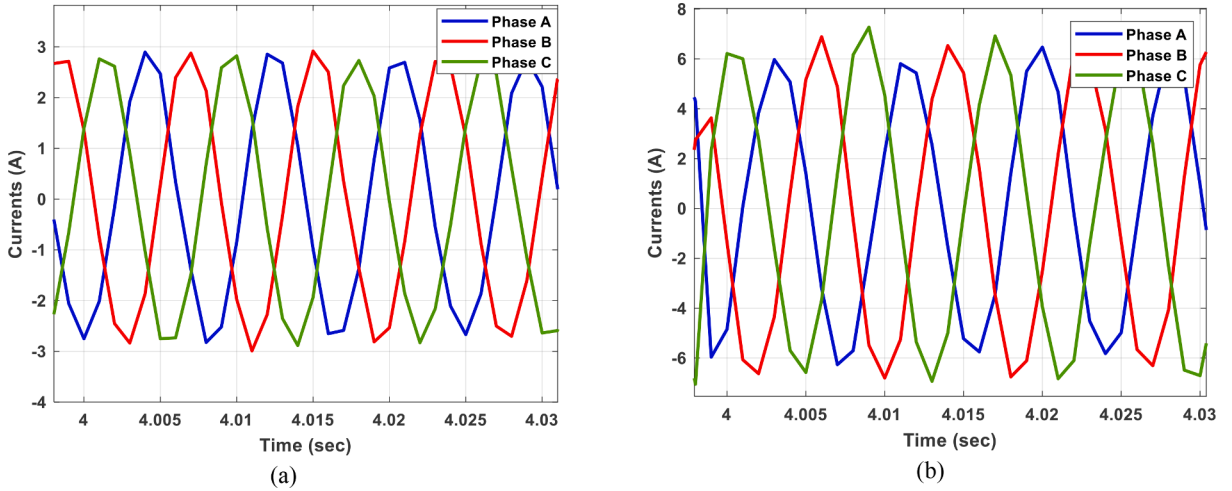


Fig. 4. The three-phase currents of PMSM in: (a) healthy state, and (b) demagnetisation fault state, running at 1800 rpm/0.4 Nm load.

because of the expensive testing and validation costs. In this work, three experiments were conducted: (1) stator inter-turn short circuit faults (ITSC); (2) no-uniform demagnetisation faults (DMF); and (3) static eccentricity faults (SEF). Figs. 2a and 2b depict the system schematic and experimental setup employed for distinct fault types. Three identical PMSMs were used in the experiments. These motors' stators, rotors, bearing, and housing are all interchangeable [23].

Table 1 lists the electrical and mechanical characteristics of the test motor driver used in the experiment. Additionally, Table 2 depicts the motors' test conditions [39]. The stator current signals of the healthy and faulty PMSMs were recorded and pre-processed using a MATLAB environment. Before extracting the diagnostic characteristics, the pre-processing phase involves eliminating the outlier and normalising the stator currents of the PMSM.

Experiment 1. : The PMSM's stator winding was distributed with 16 series turns stranded with eight conductors. For ITSCF experiment purposes, one of the 16 turns was connected to the test terminal. Fig. 3 shows the test motor's windings. First, only one conductor accessible in A2 and A3 was connected, resulting in a one-conductor fault. Then, in the same way, a two-conductor fault was formed. Short circuit current was measured in both cases under various torque and speed conditions because it directly indicates fault severity [39]. Thus, the short circuit current can be used to extract the fault features to detect the ITSCF and its severity.

Experiment 2. : A non-uniform demagnetisation fault has now been established on a test motor. For this reason, one magnet was separated from the rotor and exposed to intense heat until it demagnetised. Experiments on the speed and torque values shown in Table 2 were conducted. A single defective magnet on the rotor causes torque oscillations at mechanical rotational frequency. The speed controller compensates for torque fluctuations in speed control mode by altering motor phase currents. Fig. 4a and b illustrate the three-phase currents of the healthy state of PMSM and the PMSM with a non-uniform demagnetisation fault state, respectively. As a result, the fault's impacts on phase currents can be deployed to extract the fault features in this scenario [39].

Experiment 3. : The effects of SEF on the motor signals were studied. For this reason, the inner part of the motor cage was lathed 0.5 mm on one side, and a shim was inserted on the other. A 0.5 mm displacement to 28 percent SEF was due to the 1.8 mm air gap [39]. The tests listed in Table 2 were performed. A non-uniform air-gap clearance resulted from the rotor's displacement from the stator's

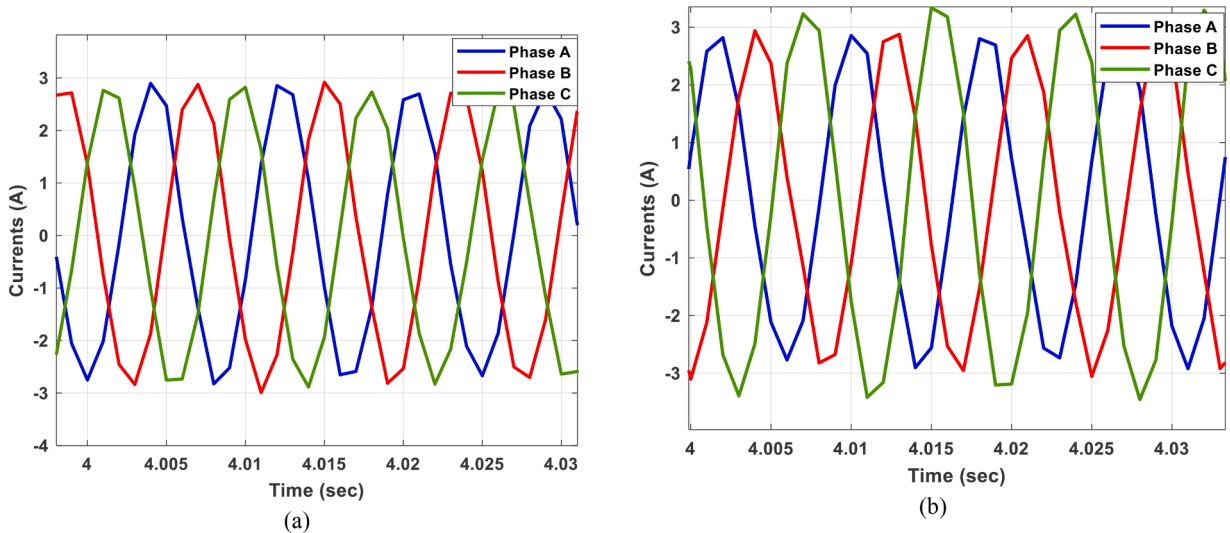


Fig. 5. Three-phase currents of the PMSM in: (a) healthy state, and (b) static eccentricity fault state, running at 1800 rpm/0.4 Nm load.

centre. Variations in phase inductances are caused by non-uniform air-gap distribution. In the case of SEF, inductance changes disrupt the motor's three-phase balance, causing phase currents to diverge. Figs. 5a and 5b show the phase currents of healthy and faulty motors running at 1800 rpm with a 0.4 Nm load. The peak value of phase current C was larger for the malfunctioning PMSM because the machined part of the bearing is close to phase-C winding.

4. Results and discussion

4.1. Feature extraction results

Feature extraction of the current phase signals of PMSM based on the VMD-HHT-CNN method for fault detection and diagnosis was conducted. The measured stator current signal at different operating conditions was decomposed using VMD, as shown in Fig. 6. The VMD approach decomposes the input current signal into five principal IMF regions. In the decomposed signal, the IMF1, IMF2, and IMF3 show the high-frequency components of the current signal, and IMF4 and IMF5 show the low-frequency components of the current signal. Fig. 6 plots the measured time-domain stator current signal and corresponding VMD-based decomposed signal IMF1 to IMF5 for (a) healthy condition, (b) short circuit condition, (c) demagnetisation condition, and (d) static eccentricity condition. Fig. 7 plots the corresponding frequency spectrum for input and decomposed signal.

The analysis of the decomposed IMFs determined that the high-frequency components, such as IMF1, exhibit fault features and correlate with different types of faults. This conclusion is based on the comparative analysis between the healthy and faulty decomposed signals, i.e., IMF1 to IMF5. Consider the IMF1 for a healthy signal, which shows the frequency peaks between 400 Hz and 460 Hz. The corresponding IMF1 frequency peaks for short circuit faults and demagnetisation faults show a clear shift for these peaks to 250 Hz and 150 Hz, respectively. However, the corresponding IMF1 of the static eccentricity fault shows little shift in frequency but some difference in peak energy. The IMF2 for the healthy signal shows frequency peaks around 100 Hz—the corresponding IMF2 frequency peaks for a short circuit fault. Demagnetisation faults and static eccentricity conditions show no clear shift in frequency peaks and are centred around 100 Hz as per the healthy IMF2 spectrum.

Similarly, the frequency spectrum of the IMF3, IMF4, and IMF5 components do not show a strong indicator or signature for the fault type when the PMSM operating state moves from a healthy to faulty state. IMF1 shows a strong correlation between a healthy to faulty state. Therefore, in this paper, only IMF1 was selected for feature extraction using HHT. Moreover, selecting a specific IMF reduces the complexity and computation and improves the accuracy of the fault detection mechanism in PMSM.

EMD was also applied to the current signal to compare its performance with VMD. We present only a limited analysis based on EMD here to evidence the results clearly. Fig. 8 plots the measured time-domain stator current signal (I_a) and corresponding EMD-based decomposed signal IMF1 to IMF7 for (a) healthy condition and (b) short circuit condition. Fig. 8c and d plot the corresponding frequency spectrum for the decomposed signal. The decomposed signal spectrum clearly shows no frequency shifting from healthy to faulty signal. The EMD method decomposed the current signal into seven IMFs regions, while the VMD decomposed the same current signal into five IMF regions; thus, the calculation scale and calculation time are reduced by the VMD method. Further analysis of decomposed EMD signal shows no clear difference between the IF feature of the healthy and faulty signal, as seen in the case of the VMD decomposed signal. Therefore, it can be concluded that the VMD-based feature extraction for the faulty signal is significantly better than the EMD-based feature extraction. Similar conclusions were also reached for the empirical wavelet transform.

As concluded above, the IMF1 from VMD decomposition shows the faulty signal's characteristics and frequency shifts. Therefore, the IMF1 was selected for the calculation of the instantaneous frequency (IF) of the PMSM at different operating states using the HHT

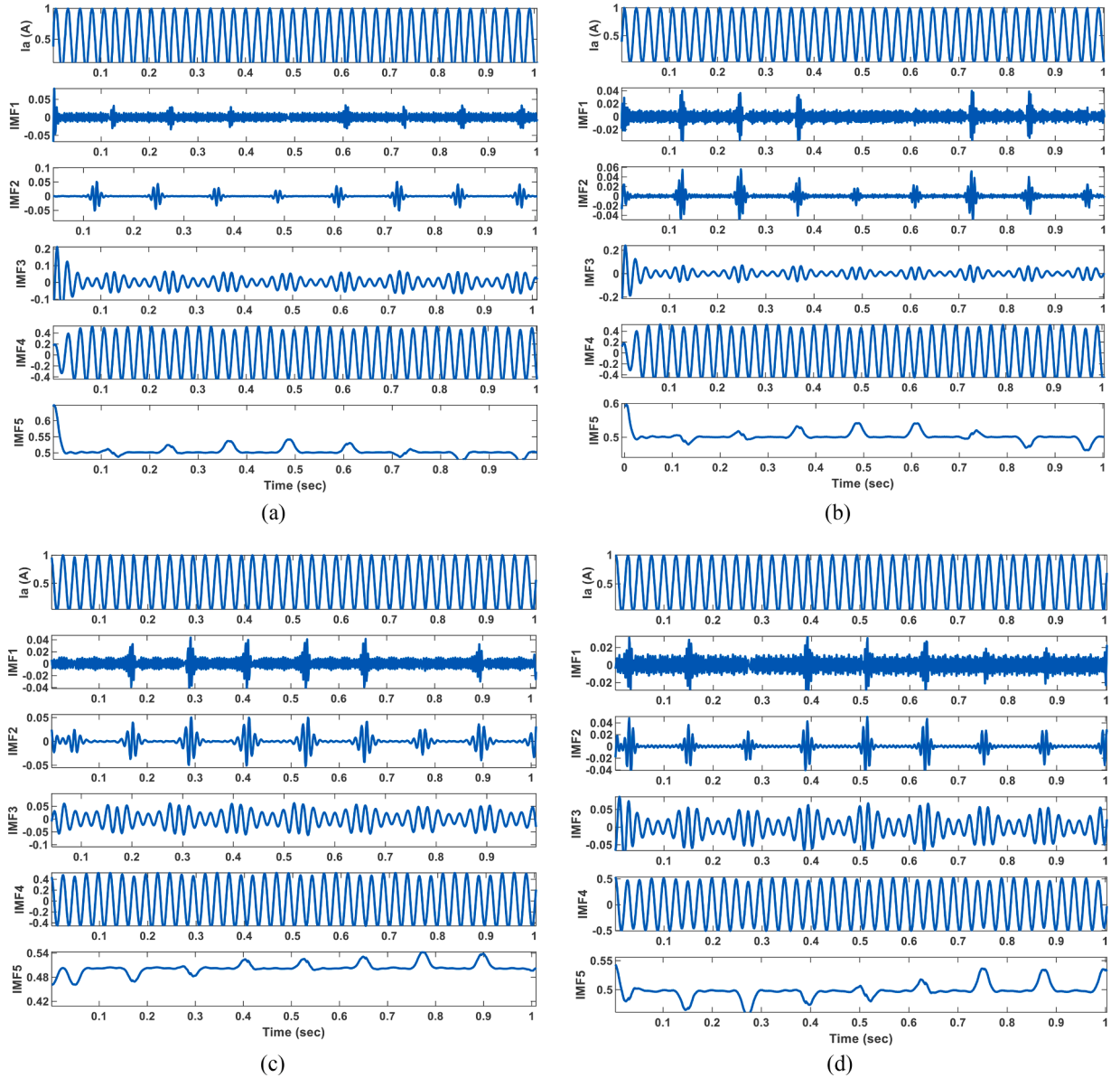


Fig. 6. VMD results of the PMSM running at 1200 rpm and 0.4 NM load torque: (a) healthy state, (b) short circuit state, (c) demagnetisation state, and (d) static eccentricity state.

algorithm (see (12) and (13)). Fig. 9 shows the spectrogram of calculated IFs for PMSM-stator phase current (I_a) under the four operational states (healthy, short-circuit, demagnetisation and static eccentricity) running at a speed of 1200 and torque of 0.4 NM. Fig. 9a shows that the IF energy is concentrated around 430 Hz for the healthy current signal. The IF has shifted to 230 Hz for the short circuit fault condition.

Similarly, the IF energy for the demagnetisation fault condition is concentrated around 150 Hz. The IF energy for static eccentricity fault is concentrated around 405 Hz, which is closer to the IF energy concentration for the healthy current signal of 430 Hz. The same features can be observed for other data collected under different operational conditions. From this analysis, it was concluded that the IF signature extracted using VMD-HHT can be used as a feature for fault detection of the PMSM under various operating conditions. The apparent frequency shifting of VMD-HHT based IF between the healthy and faulty PMSM provides a robust diagnostic tool for monitoring electric machines and predictive maintenance. Using advanced machine learning to design a fully autonomous and online fault diagnostic system, this method has been extended.

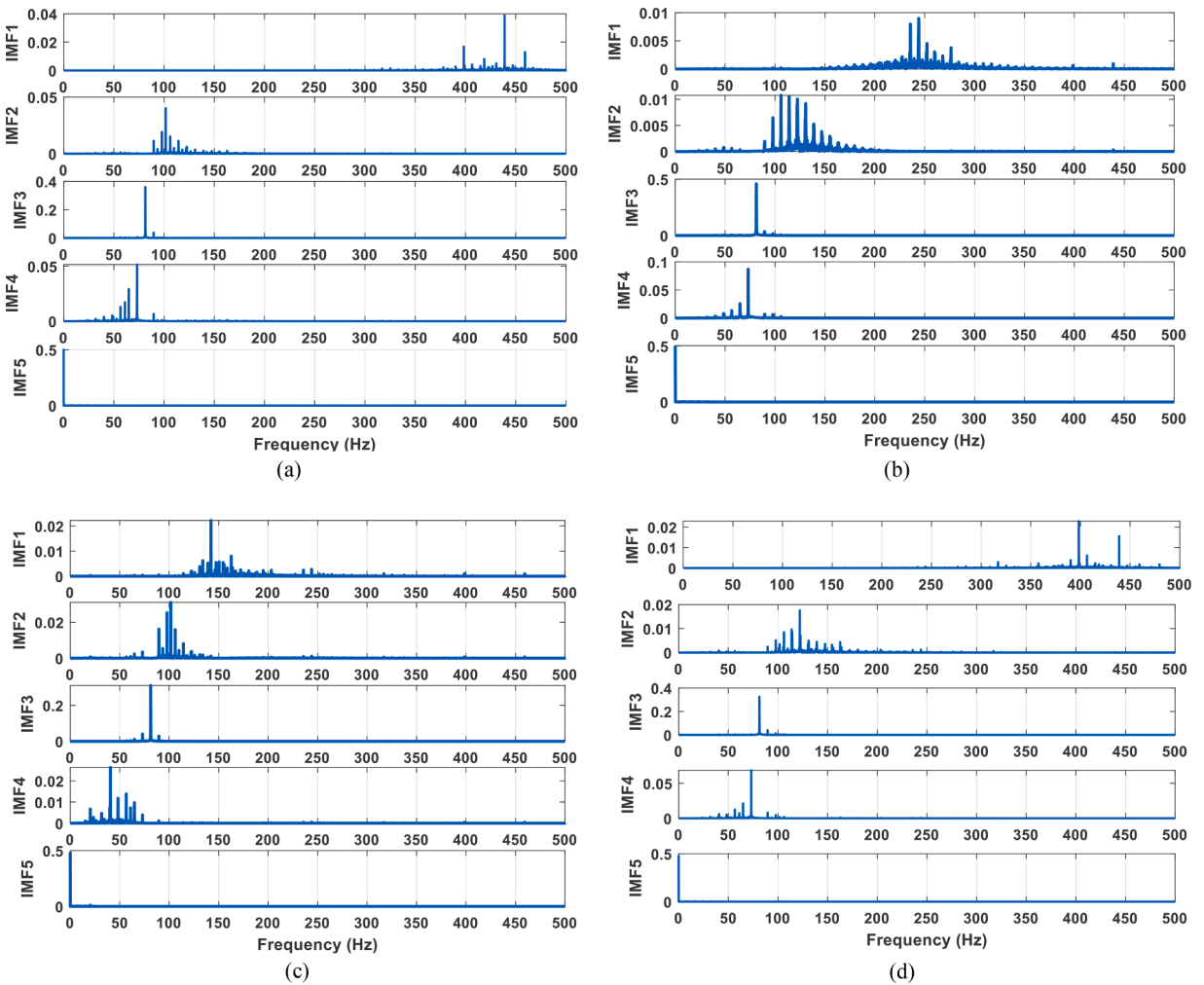


Fig. 7. The frequency spectrum of each IMF in: (a) healthy condition, (b) short-circuit fault condition, (c) demagnetisation fault condition, and (d) static eccentricity fault condition.

4.2. Autonomous fault detection and diagnosis system

After the IFs are extracted in the VMD-HHT step, the IFs are fed into 1-D CNN networks for fault detection and diagnosis. In reality, the fault detection process is a binary classification utilising the CNN model that distinguishes between healthy and faulty states. The simplified system is based on VMD-HHT decomposition phase currents signals, IMF selection, extraction of IF feature using HHT and training through CNN for autonomous fault detection, as shown in Fig. 1. The extracted IF feature as described above is then split into training (70%) and testing (30%) datasets for each operating condition of the PMSM to train and test the accuracy of the proposed CNN models. Table 3 illustrates the fault type of the PMSM and the corresponding class label used to train the developed CNN.

Data preparation is crucial since it improves learning quality by enlarging data size and enhancing fault detection robustness in a noisy environment. The same proposed CNN model was employed for the fault diagnosis process but with a difference in the last classification layer. In the fault detection process (Fig. 10), the last layer in the proposed CNN model is allocated for binary classification (healthy or faulty). When the fault detection CNN network detects the fault, the fault diagnosis process is switched on. To assess the accuracy of the trained CNN, the detection and diagnosis accuracy index (C_{acc}) is expressed as:

$$C_{acc} = \frac{Y_c}{Y_c + Y_m} \cdot 100\% \quad (19)$$

Where Y_c is the number of correct prediction states, and Y_m is the number of misclassifications. This accuracy index is applied for both the detection and diagnosis state of the PMSM.

Figs. 11a and 11b show the architecture of the proposed CNN model for fault detection and diagnosis of the PMSM, respectively. The proposed CNN model consists of two convolutional layers with a kernel size of ten and filter sizes of 100 and 50 for the first and

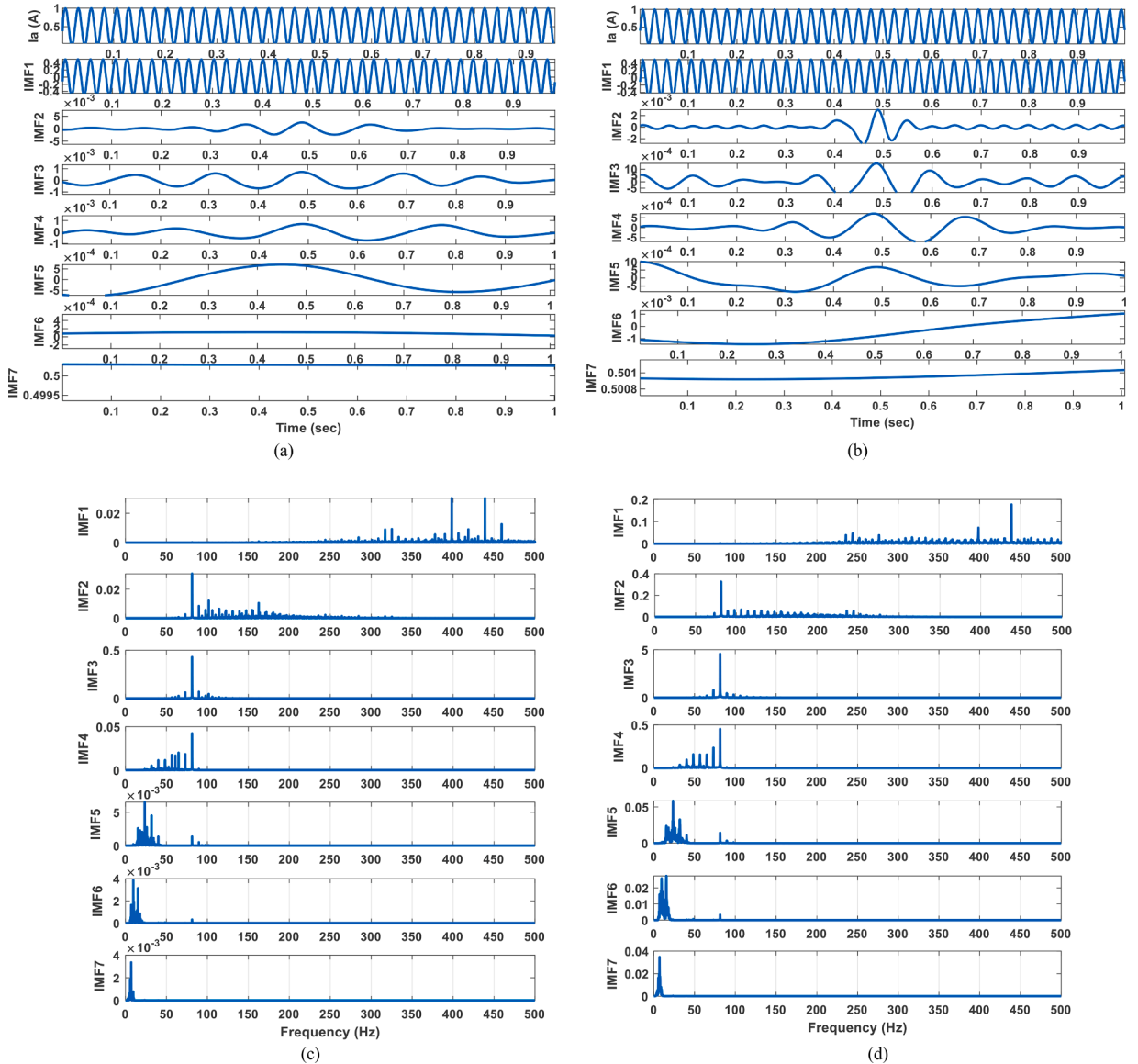


Fig. 8. EMD results of the PMSM running at 1200 rpm and 0Nm load torque: (a) healthy condition, (b) short-circuit fault condition, (c) the frequency spectrum of the healthy PMSM, and (c) the frequency spectrum of short-circuit PMSM.

second convolutional layers—two max-pooling layers with a pool size of two for down sampling and compressing helpful information. A flattening layer arranges the features into a vector and fully connected layers with a ReLU activation function. Finally, the classification layer was also designed to classify the extracted feature.

Once the training process is completed using 70% of the dataset for each operating condition, the trained CNN model was tested using the testing dataset. The proposed fault detection CNN model successfully and efficiently discriminates between healthy and faulty states of the PMSM working at different operating conditions (see Table 2) with 100% detection accuracy. Fig. 12 illustrates the confusion matrices for the fault detection result of the PMSM at four operating conditions: 600 rpm-0Nm, 1200 rpm- 0.8Nm, 1800 rpm- 1.2Nm, and 2400 rpm- 0.4Nm. The results obtained from the developed CNN validate this highly effective proposed solution, mainly due to the use of the VMD method in removing the useless IMFs common to healthy and faulty states, as well as the HHT technique for extracting the IF feature. Moreover, the results show the capability of the CNN to learn to distinguish between the healthy and faulty IF features of the PMSM in the training process.

In terms of the fault diagnosis process, Table 4 illustrates the classification accuracy of the trained CNN model. The model was trained for each operating condition presented in Table 2. The classification accuracy of the proposed method shows highly accurate diagnosis for each fault state. To validate the performance of the proposed solution, the developed CNN was trained on the extracted IF feature using the EMD-HHT method, as shown in Table 4. Our comparison clearly demonstrates that the proposed VMD-HHT

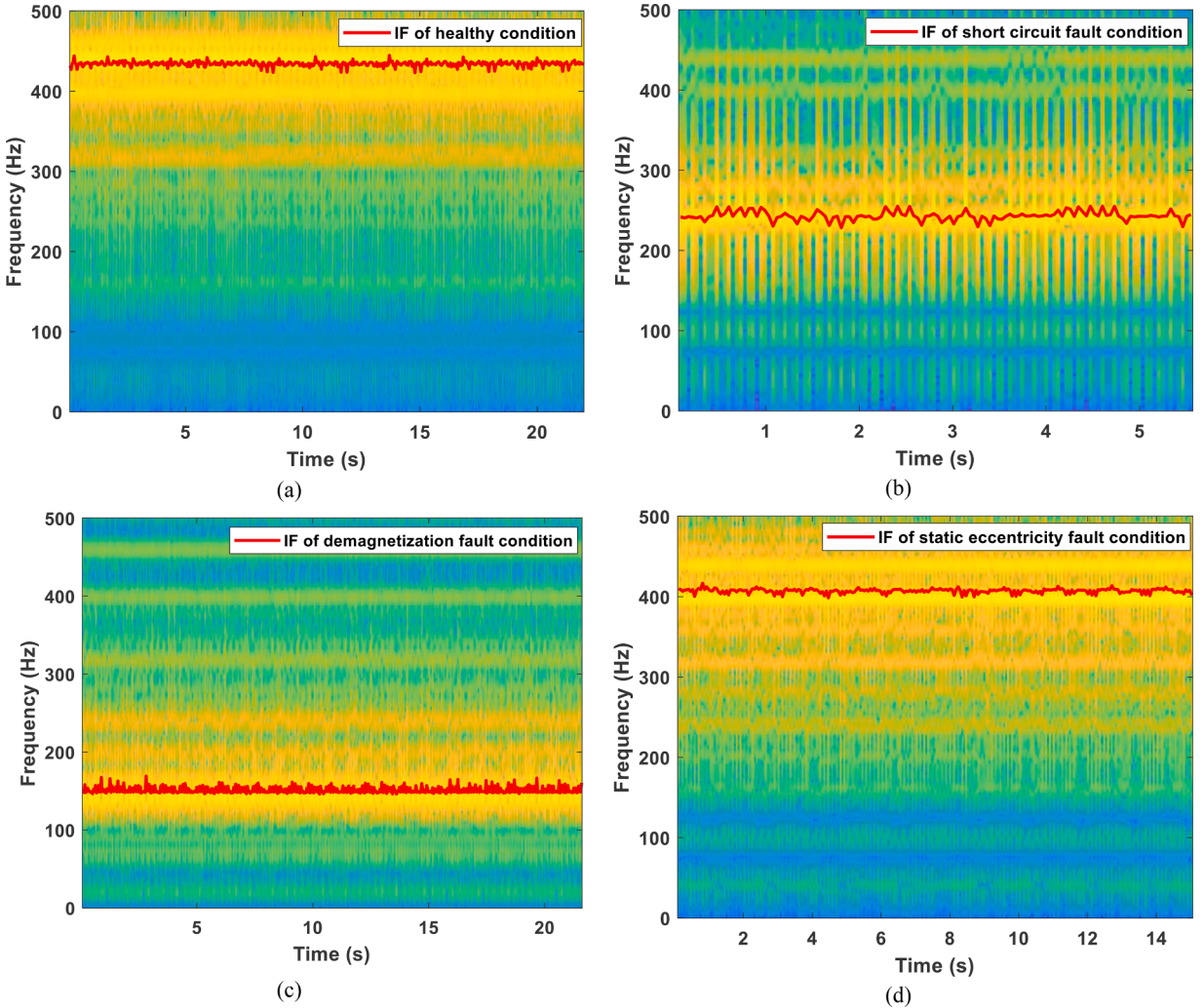


Fig. 9. Instantaneous frequency results of the PMSM running at 1200 rpm and 0Nm load torque: (a) healthy condition, (b) a short circuit fault condition, (c) a demagnetisation fault condition, and (d) a static eccentricity fault condition.

Table 3
PMSM fault types and class labels.

Fault type	Class label
3% ITSCF	F1
6% ITSCF	F2
Demagnetisation	F3
Static eccentricity	F4

technique outperforms the performance of the EMD-HHT technique due to the advantage of the VMD technique in decomposing the measured current signals into several IMFs without introducing an aliasing effect into the decomposed IMFs. In addition, it is worth noticing the ability of the proposed method to diagnose the minor ITSCF (F1) accurately, since the traditional time and frequency methods hardly distinguish this slight variation in the PMSM.

Moreover, Fig. 13 shows the diagnostic accuracy of the developed approach compared to the EMD-HHT approach under four loads (0.4 Nm, 0.8 Nm, 1.2 Nm, and 1.6 Nm) and speeds (600 rpm, 1200 rpm, 180 rpm, and 2400 rpm). Notably, the average classification accuracy in these cases is around 98.9%, while the average classification accuracy of the EMD-HHT method is approximately 85%. This classification accuracy of the EMD-HHT could broadly lead to incorrect scheduling of the maintenance of the PMSM. This means that maintenance may be performed too late or too early, which can negatively impact the ability of the PMSM to deliver its intended service. Therefore, the proposed method can effectively monitor the state of PMSM at different loads and speeds.

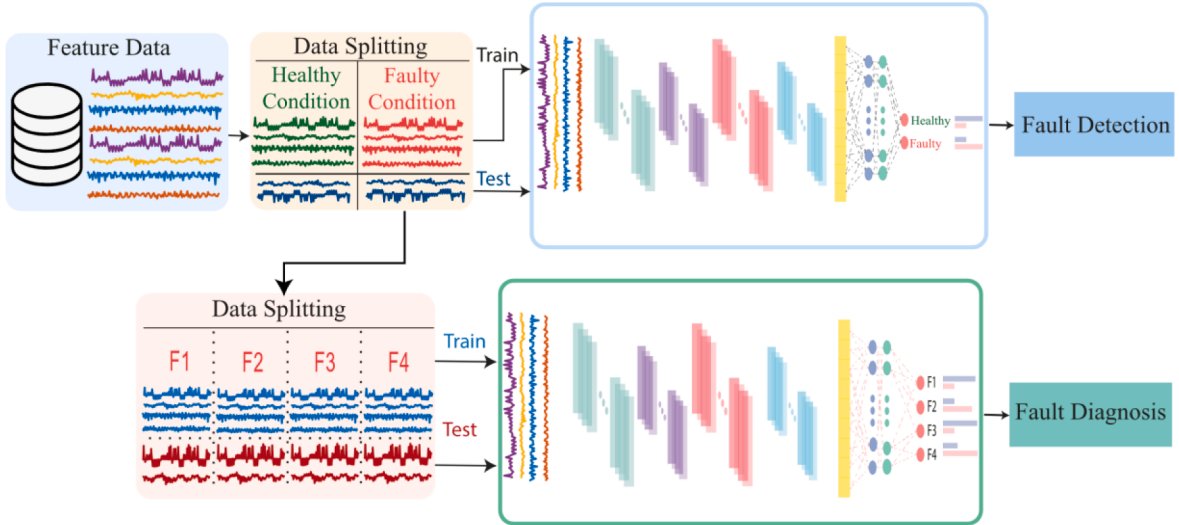


Fig. 10. Faults detection and diagnosis process.

4.3. Comparative analysis with other data-driven methods

To further confirm the superiority of the proposed method, the fault detection and diagnosis performance of the developed CNN was compared with other data-driven algorithms, in particular, with the support vector machine (SVM) and K-nearest neighbours (KNN) data-driven algorithms. The concept of these algorithms is shown in Fig. 14 and their mathematical description can be found in [24,25].

For the fault detection task, both algorithms correctly classified the tested dataset into healthy or faulty classes with 100% detection accuracy, which is similar to the performance of the proposed CNN model for the fault detection task. However, regarding the fault classification task, the proposed CNN model achieved higher classification accuracy than the SVM and KNN, as presented in Table 5.

4.4. Comparative analysis with state-of-the-art methods

To demonstrate the superiority of the proposed VMD-HHT-CNN method for fault diagnosis and detection of PMSM, it was compared with other existing methods. Table 6 presents a comparison of the proposed VMD-HHT method with other methods of fault diagnosis and detection in PMSMs. As shown in Table 6, although the existing techniques deliver excellent classification accuracy, they are limited to one or two fault types. On the other hand, the proposed VMD-HHT method has proven its generality and capacity to diagnose and detect three different fault types, which indicates the superiority of the proposed method compared to the existing state-of-the-art methods.

5. Practical implications

The proposed project has significant practical implications as it seeks to address the current limitations in fault detection and diagnosis of electrical machines. Existing techniques in the literature are limited in their ability to detect multiple types of faults from stator currents in PMSMs, often relying on fixed speed/load operating conditions and a single task of fault detection. Furthermore, few studies have investigated these approaches under various working conditions and fault diagnoses, but the detection algorithms of PMSMs are underdeveloped. This project therefore proposed an autonomous fault detection and diagnosis method that utilises VMD decomposition, IMF selection, HHT feature extraction, and two CNN models to automate fault detection and classification. The proposed system can detect and classify common failures in PMSMs, such as stator ITSC fault, non-uniform demagnetisation of permanent magnets, and static rotor eccentricities.

To the authors' knowledge, no previous work has developed a generic data-driven system for detecting and classifying faults in PMSMs. By relying solely on built-in sensors, the proposed approach is non-intrusive and does not interfere with motor operation. This feature results in improved reliability, detection accuracy, reduced maintenance costs, increased safety, better decision-making, and optimised asset management. The practical implications of this project are, therefore, far-reaching and have the potential to improve the efficiency and reliability of electrical machines, leading to a more sustainable and eco-friendly energy future. The proposed techniques have broad applications and can be adapted to various electrical machines, resulting in reduced downtime, increased efficiency, and lower environmental impact.

However, data collection can be a significant practical challenge for this data-driven approach, as obtaining sufficient data at various operating conditions and fault scenarios may be difficult. The accuracy of the data is also important as it affects the performance of the fault detection and diagnosis algorithm. Therefore, it is crucial to ensure that the sensors used for data collection are

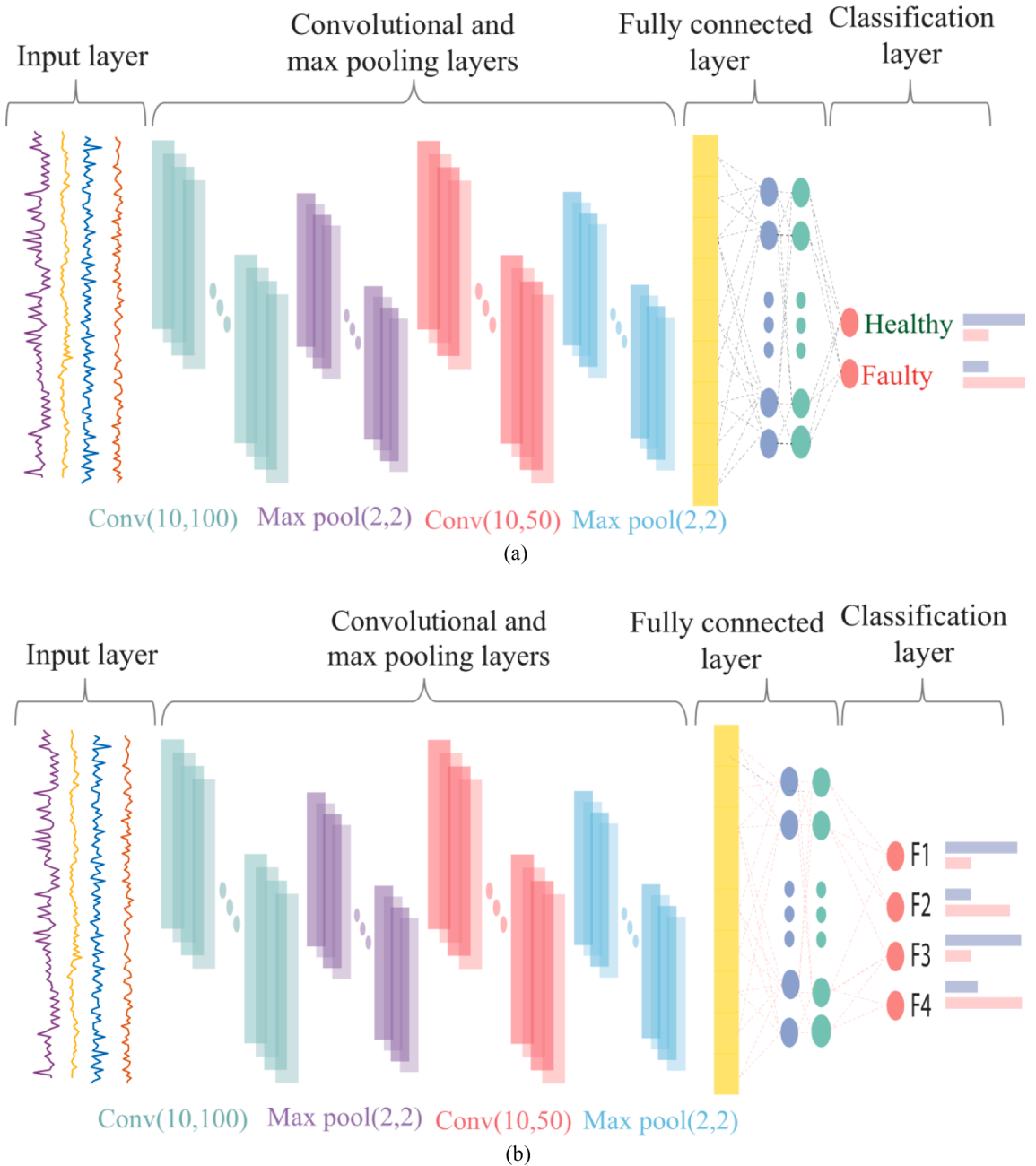


Fig. 11. The architecture of the proposed CNN for faults: (a) detection and (b) diagnosis.

calibrated and functioning properly. This point was addressed in the research and appropriate measures were taken to ensure the accuracy and representativeness of the collected data. Another issue that may arise is the possibility of data degeneracy, where the learning algorithm may overfit the data and perform poorly on new and unseen data. To address this issue, a range of operating conditions and fault scenarios were used to ensure the diversity of the training data. Furthermore, the proposed fault detection and diagnosis algorithm was validated using various performance metrics, demonstrating its effectiveness in detecting and classifying faults in PMSSMs. Overall, while data-related challenges and limitations could have arisen during the course of this work, appropriate measures were taken to ensure data accuracy, diversity, and representativeness of real-world scenarios.

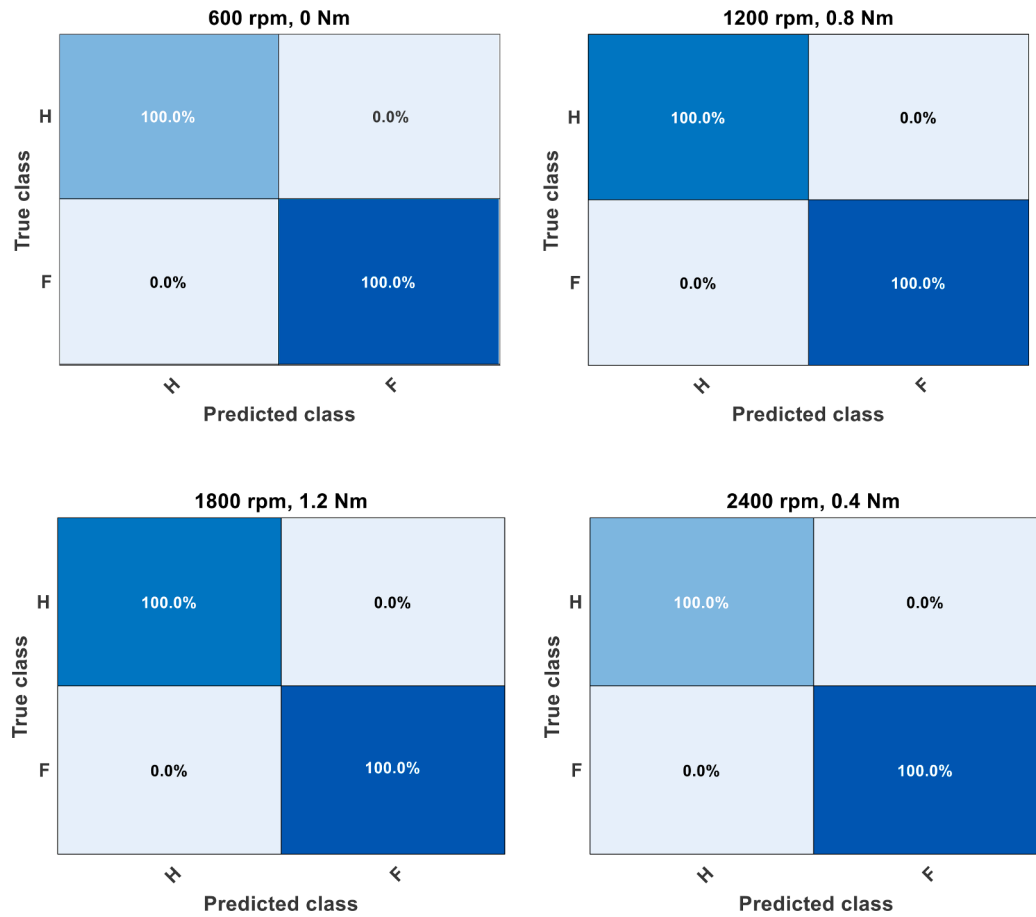


Fig. 12. Confusion matrices for the fault detection results of the PMSM under four operating conditions.

Table 4

Confusion matrix for the fault diagnosis results of PMSM working at different speeds using the VMD-HHT and EMD-HHT methods: (a–b) 600 rpm/0 NM, (c–d) 1200 rpm/0 NM, (e–f) 1800 rpm/0 NM, and (g–h) 2400 rpm/0 NM.

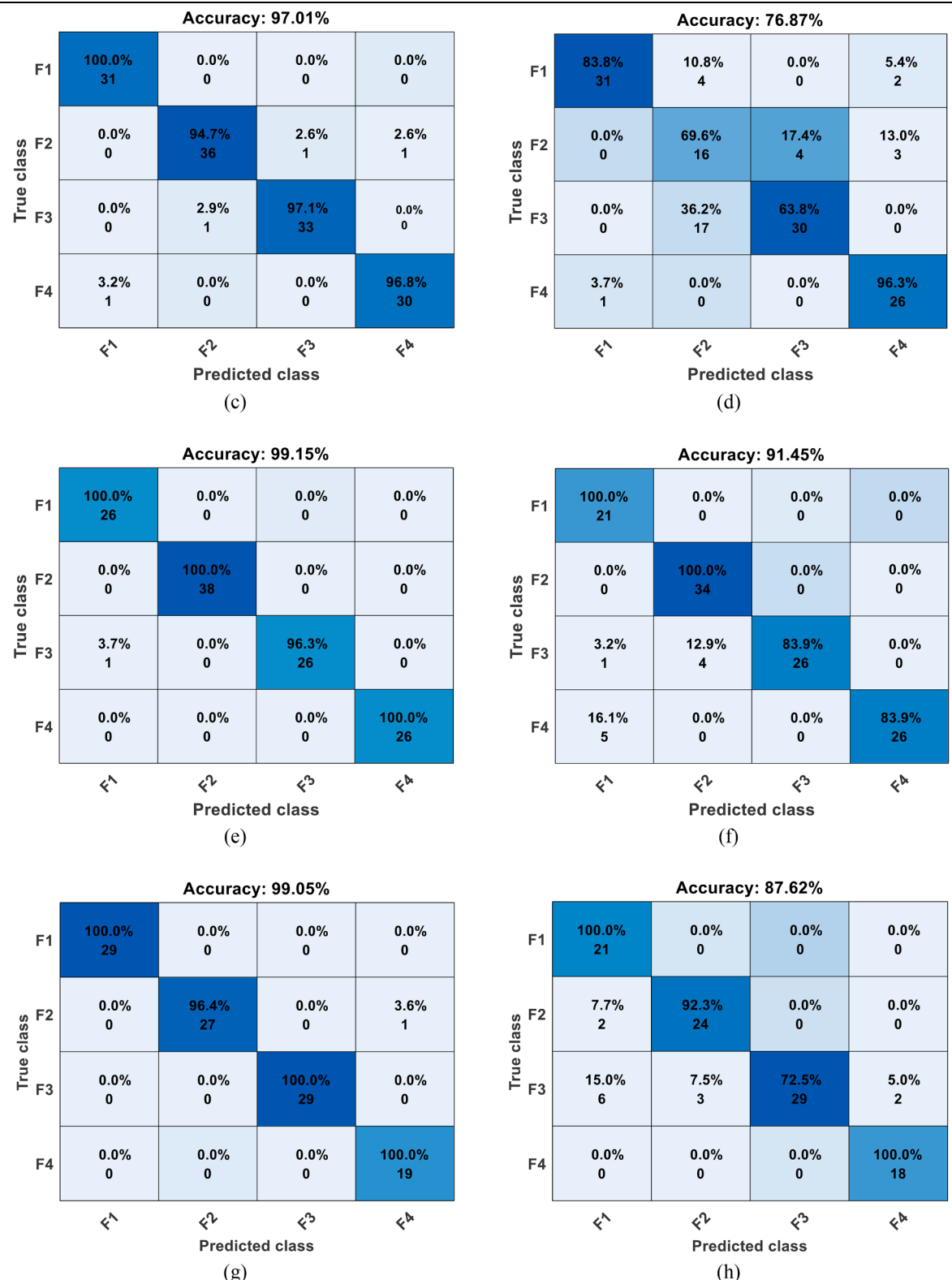
VMD-HHT					EMD-HHT					
Accuracy: 97.99%					Accuracy: 89.93%					
True class	F1	97.0% 32	0.0% 0	0.0% 0	3.0% 1	F1	100.0% 23	0.0% 0	0.0% 0	0.0% 0
	F2	0.0% 0	97.7% 43	0.0% 0	2.3% 1	F2	0.0% 0	93.5% 43	4.3% 2	2.2% 1
	F3	0.0% 0	2.3% 1	97.7% 42	0.0% 0	F3	0.0% 0	2.4% 1	95.1% 39	2.4% 1
	F4	0.0% 0	0.0% 0	0.0% 0	100.0% 29	F4	23.1% 9	0.0% 0	2.6% 1	74.4% 29
		H ¹	H ²	H ³	H ⁴		H ¹	H ²	H ³	
		Predicted class					Predicted class			

(a)

(b)

(continued on next page)

Table 4 (continued)



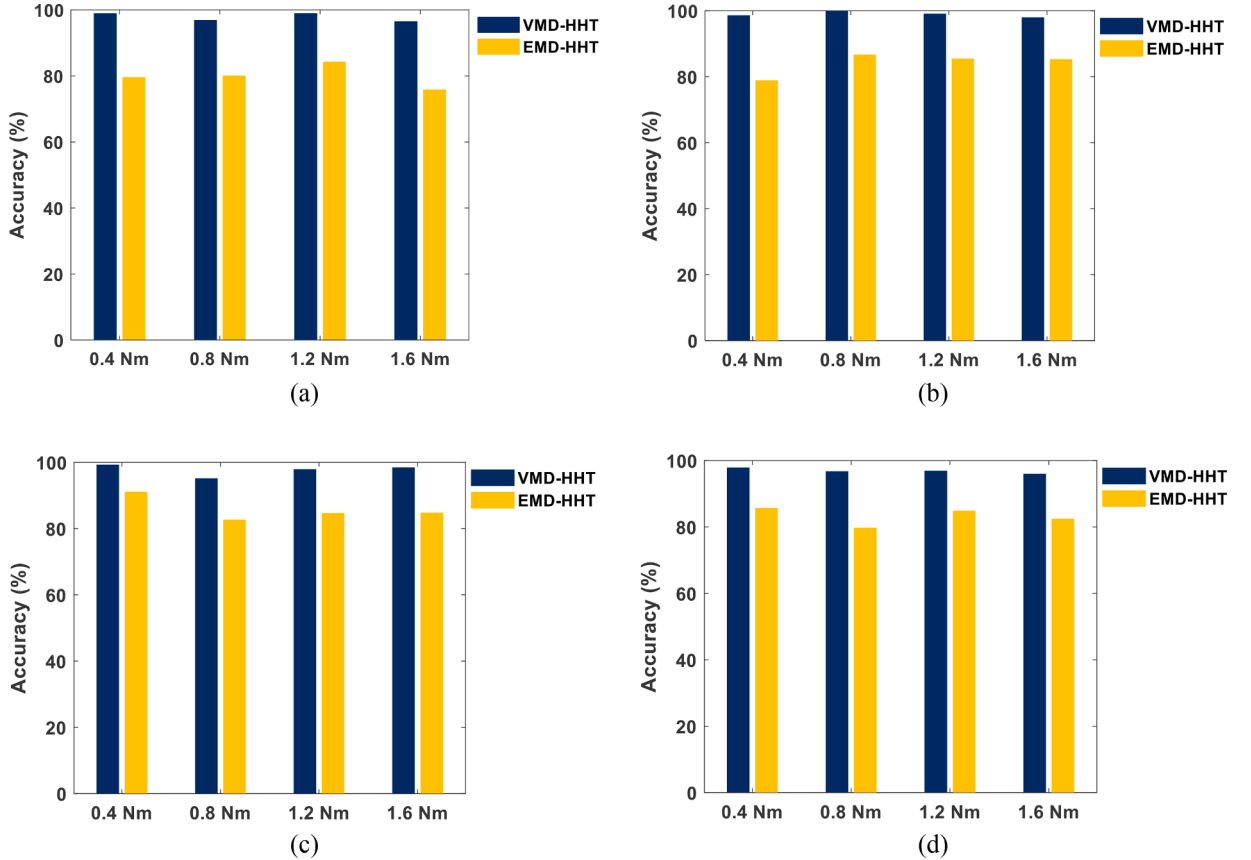


Fig. 13. Fault diagnostic results of the PMSM working at different load torque and speeds: (a) PMSM at 600 rpm, (b) at 1200 rpm, (c) at 1800 rpm, and (d) at 2400 rpm.

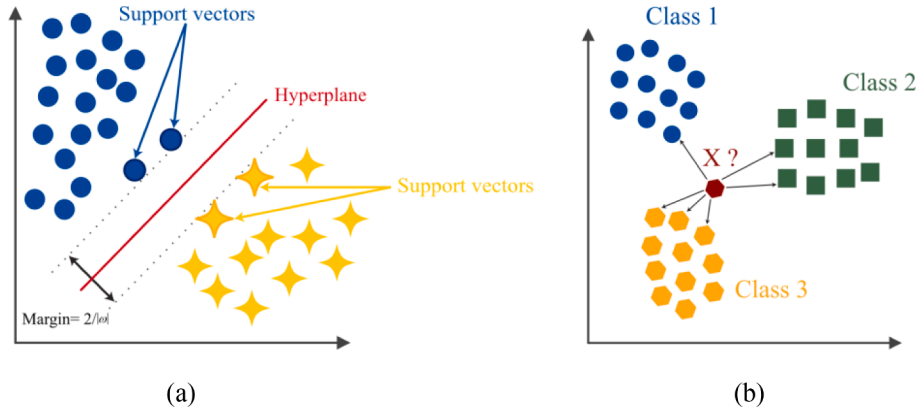


Fig. 14. Overview of the concept of SVM and KNN algorithms.

6. Conclusion

A novel condition monitoring and fault detection paradigm for electrical machines has been investigated and presented in this paper. The proposed technique coupled the VMD, HHT and CNN methods for the accurate detection of three types of faults in PMSMs: ITSCF, non-uniform DEF, and SEF. The faults on the motors under test were artificially seeded, and the proposed technique was validated against measured data. The proposed method is non-invasive and has the advantage of using only built-in sensors; the stator

Table 5

Confusion matrix for the fault diagnosis results of the PMSM working at different speeds using the SVM and KNN methods: (a–b) 600 rpm/0 Nm, (c–d) 1200 rpm/0 NM, (e–f) 1800 rpm/0 NM, and (g–h) 2400 rpm/0 NM.

SVM					KNN					
True class	Accuracy: 95.30%				Accuracy: 89.26%					
	F1	96.8% 30	3.2% 1	0.0% 0	0.0% 0	F1	100.0% 22	0.0% 0	0.0% 0	0.0% 0
	F2	0.0% 0	100.0% 41	0.0% 0	0.0% 0	F2	0.0% 0	93.5% 43	4.3% 2	2.2% 1
	F3	4.2% 2	4.2% 2	87.5% 42	4.2% 2	F3	0.0% 0	2.4% 1	95.1% 39	2.4% 1
	F4	0.0% 0	0.0% 0	0.0% 0	100.0% 29	F4	25.0% 10	0.0% 0	2.5% 1	72.5% 29
Predicted class					Predicted class					
(a)										
True class	Accuracy: 93.28%				Accuracy: 95.52%					
	F1	100.0% 31	0.0% 0	0.0% 0	0.0% 0	F1	93.9% 31	0.0% 0	0.0% 0	6.1% 2
	F2	2.2% 1	80.4% 37	8.7% 4	8.7% 4	F2	2.4% 1	90.2% 37	2.4% 1	4.9% 2
	F3	0.0% 0	0.0% 0	100.0% 30	0.0% 0	F3	0.0% 0	0.0% 0	100.0% 33	0.0% 0
	F4	0.0% 0	0.0% 0	0.0% 0	100.0% 27	F4	0.0% 0	0.0% 0	0.0% 0	100.0% 27
Predicted class					Predicted class					
(b)										
True class	Accuracy: 91.45%				Accuracy: 85.47%					
	F1	96.3% 26	0.0% 0	3.7% 1	0.0% 0	F1	100.0% 27	0.0% 0	0.0% 0	0.0% 0
	F2	0.0% 0	100.0% 30	0.0% 0	0.0% 0	F2	0.0% 0	96.4% 27	3.6% 1	0.0% 0
	F3	3.8% 1	0.0% 0	96.2% 25	0.0% 0	F3	0.0% 0	4.8% 1	95.2% 20	0.0% 0
	F4	0.0% 0	23.5% 8	0.0% 0	76.5% 26	F4	0.0% 0	24.4% 10	12.2% 5	63.4% 26
Predicted class					Predicted class					
(c)										
True class	Accuracy: 95.30%				Accuracy: 89.26%					
	F1	96.8% 30	3.2% 1	0.0% 0	0.0% 0	F1	100.0% 22	0.0% 0	0.0% 0	0.0% 0
	F2	0.0% 0	100.0% 41	0.0% 0	0.0% 0	F2	0.0% 0	93.5% 43	4.3% 2	2.2% 1
	F3	4.2% 2	4.2% 2	87.5% 42	4.2% 2	F3	0.0% 0	2.4% 1	95.1% 39	2.4% 1
	F4	0.0% 0	0.0% 0	0.0% 0	100.0% 29	F4	25.0% 10	0.0% 0	2.5% 1	72.5% 29
Predicted class					Predicted class					
(d)										
True class	Accuracy: 93.28%				Accuracy: 95.52%					
	F1	100.0% 31	0.0% 0	0.0% 0	0.0% 0	F1	93.9% 31	0.0% 0	0.0% 0	6.1% 2
	F2	2.2% 1	80.4% 37	8.7% 4	8.7% 4	F2	2.4% 1	90.2% 37	2.4% 1	4.9% 2
	F3	0.0% 0	0.0% 0	100.0% 30	0.0% 0	F3	0.0% 0	0.0% 0	100.0% 33	0.0% 0
	F4	0.0% 0	0.0% 0	0.0% 0	100.0% 27	F4	0.0% 0	0.0% 0	0.0% 0	100.0% 27
Predicted class					Predicted class					
(e)										
True class	Accuracy: 91.45%				Accuracy: 85.47%					
	F1	96.3% 26	0.0% 0	3.7% 1	0.0% 0	F1	100.0% 27	0.0% 0	0.0% 0	0.0% 0
	F2	0.0% 0	100.0% 30	0.0% 0	0.0% 0	F2	0.0% 0	96.4% 27	3.6% 1	0.0% 0
	F3	3.8% 1	0.0% 0	96.2% 25	0.0% 0	F3	0.0% 0	4.8% 1	95.2% 20	0.0% 0
	F4	0.0% 0	23.5% 8	0.0% 0	76.5% 26	F4	0.0% 0	24.4% 10	12.2% 5	63.4% 26
Predicted class					Predicted class					
(f)										

(continued on next page)

Table 5 (continued)

Accuracy: 99.05%					Accuracy: 96.19%						
True class	F1	96.7% 29	0.0% 0	3.3% 1	0.0% 0	F1	93.3% 28	6.7% 2	0.0% 0	0.0% 0	
	F2	0.0% 0	100.0% 27	0.0% 0	0.0% 0	F2	0.0% 0	96.2% 25	0.0% 0	3.8% 1	
	F3	0.0% 0	0.0% 0	100.0% 28	0.0% 0	F3	0.0% 0	0.0% 0	100.0% 29	0.0% 0	
	F4	0.0% 0	0.0% 0	0.0% 0	100.0% 20	F4	5.0% 1	0.0% 0	0.0% 0	95.0% 19	
	Predicted class				Predicted class						
(g)					(h)						

Table 6

Comparison of the VMD-HHT method with existing methods.

Method	Classifier	Fault type	Accuracy
Instantaneous current residual map (ICRM) [8]	CNN	ITSCF and Misalignment	94.9%
VMD-Energy [19]	FCM-PNN	ITSCF and DEF	95%
Signal-to-image conversion [26]	VGG-16	DEF and bearing	96.6%
Conditional generative adversarial net (CGAN) [27]	OSAE	ITSCF	98.9%
VMD-HBS [20]	ResNet-101	Bearing	94%
VMD-HHT (proposed)	CNN	ITSCF, DEF, and SEF	98.8%

phase current signals of the PMSM were captured and analysed only to detect the three faults listed above. The fault detection strategy was developed by combining VMD, HHT and CNN. The VMD was first applied to the stator phase current signals to analyse the characteristic behaviour of the current signals by decomposing the current signals into several IMFs. These IMFs between the healthy and faulty signals were compared to select the one with the frequency shift characteristics. The HHT method was used to extract the instantaneous frequency feature from the decomposed stator phase current, which was subsequently delivered to the CNN algorithm with a prediction accuracy of 98.8%. Two machine learning methods were developed to compare and validate the performance of the developed CNN model, including SVM and KNN, although CNN has proven to provide more significant detection and classification accuracy at 98.8%, compared to 95% for the SVM and 96.8% for KNN models. Moreover, the proposed method was compared to existing approaches in the field, such as EMD, and we found that the VMD plus HHT offered accurate diagnosis features. Lastly, the proposed method was validated against recent techniques published in the literature, and again the results demonstrated the effectiveness of the proposed method for the detection and diagnosis of three different types of faults in PMSMs.

CRediT authorship contribution statement

Ma'd El-Dalahmeh: Conceptualization, Methodology, Software, Writing – original draft, Validation. **Maher Al-Greer:** Investigation, Supervision, Conceptualization, Writing – review & editing, Formal analysis, Validation. **Imran Bashir:** Investigation, Methodology, Writing – review & editing, Validation. **Mo'ath El-Dalahmeh:** Software, Writing – original draft. **Aykut Demirel:** Validation, Data curation. **Ozan Keysan:** Validation, Data curation.

Declaration of Competing Interest

The authors declare that they have no known competing financial interests or personal relationships that could have influenced the work reported in this paper.

Data availability

Data will be made available on request.

Acknowledgements

This work was supported by the Lloyd's Register Foundation under Project No. [Sg2\100005]. We would also like to thank Aselsan (Aykut Demirel) for the experimental setup and sharing the motor data.

References

- [1] Orlowska-Kowalska T, Wolkiewicz M, Pietrzak P, Skowron M, Ewert P, Tarchala G, Krzysztofiak M, Kowalski CT. Fault diagnosis and fault-tolerant control of PMSM drives-state of the art and future challenges. *IEEE Access* 2022.
- [2] Prasanth A. Certain investigations on energy-efficient fault detection and recovery management in underwater wireless sensor networks. *J Circ Syst Comput* 2021;30(08):2150137.
- [3] Chen Y, Liang S, Li W, Liang H, Wang C. Faults and diagnosis methods of permanent magnet synchronous motors: a review. *Appl Sci* 2019;9(10):2116.
- [4] Alvarez-Gonzalez F, Griffó A, Wang B. Permanent magnet synchronous machines inter-turn short circuit fault detection by means of model-based residual analysis. In: IECON 2018 - 44th annual conference of the IEEE industrial electronics society; 2018. p. 647–52.
- [5] Bouzid MBK, Champenois G, Maalaoui A, Tnani S. Efficient simplified physical faulty model of a permanent magnet synchronous generator dedicated to the stator fault diagnosis Part I: faulty model conception. *IEEE Trans Ind Appl* 2017;53(3):2752–61.
- [6] Lee H, Jeong H, Koo G, Ban J, Kim SW. Attention recurrent neural network-based severity estimation method for interturn short-circuit fault in permanent magnet synchronous machines. *IEEE Trans Ind Electron* 2021;68(4):3445–53.
- [7] Hang J, Shu X, Ding S, Huang Y. Robust open-circuit fault diagnosis for PMSM drives using wavelet convolutional neural network with small samples of normalized current vector trajectory graph. *IEEE Trans Ind Electron* 2023.
- [8] Park CH, Kim H, Suh C, Chae M, Yoon H, Youn BD. A health image for deep learning-based fault diagnosis of a permanent magnet synchronous motor under variable operating conditions: instantaneous current residual map. *Reliabil Eng Syst Saf* 2022;226:108715.
- [9] Quiroz JC, Mariun N, Mehrjou MR, Izadi M, Misron N, Mohd Radzi MA. Fault detection of broken rotor bar in LS-PMSM using random forests. *Measurement* 2018;116:273–80.
- [10] Pietrzak P, Wolkiewicz M. On-line detection and classification of PMSM stator winding faults based on stator current symmetrical components analysis and the knn algorithm. *Electronics* 2021;10(15):1786.
- [11] Hang J, Zhang J, Xia M, Ding S, Hua W. Interturn fault diagnosis for model-predictive-controlled-PMSM based on cost function and wavelet transform. *IEEE Trans Power Electron* 2020;35(6):6405–18.
- [12] Ribeiro Junior RF, dos Santos Areias IA, Campos MM, Teixeira CE, da Silva LEB, Gomes GF. Fault detection and diagnosis in electric motors using convolution neural network and short-time Fourier transform. *J Vib Eng Technol* 2022;1–12.
- [13] Zanardelli WG, Strangas EG, Aviyente S. Identification of intermittent electrical and mechanical faults in permanent-magnet ac drives based on time-frequency analysis. *IEEE Trans Ind Appl* 2007;43(4):971–80.
- [14] Liu D, Cheng W, Wen W. Rolling bearing fault diagnosis via STFT and improved instantaneous frequency estimation method. *Procedia Manuf* 2020;49:166–72.
- [15] Sadeghi R, Samet H, Ghanbari T. Detection of stator short-circuit faults in induction motors using the concept of instantaneous frequency. *IEEE Trans Ind Inform* 2018;15(8):4506–15.
- [16] Zhang J, Tounzi A, Benabou A, Le Menach Y. Detection of magnetization loss in a PMSM with Hilbert Huang transform applied to non-invasive search coil voltage. *Math Comput Simul* 2021;184:184–95.
- [17] Zhang Q, Ma W, Li G, Ding J, Xie M. Fault diagnosis of power grid based on variational mode decomposition and convolutional neural network. *Electric Power Syst Res* 2022;208:107871.
- [18] Zhao S, Chen Y, Rehman AU, Liang F, Wang S, Zhao Y, Deng W, Ma Y, Cheng Y. The inter-turns short circuit fault detection based on external leakage flux sensing and VMD-HHT analytical method for DFIG. In: 2021 International conference on sensing, measurement & data analytics in the era of artificial intelligence (ICSMID); 2021. p. 1–5.
- [19] Dai X, Zhang Y, Qiao L, Sun D. Fault diagnosis of permanent magnet synchronous motor based on improved probabilistic neural network. In: 2021 40th Chinese control conference (CCC); 2021. p. 2767–72.
- [20] Lin S-L. Application combining vmd and resnet101 in intelligent diagnosis of motor faults. *Sensors* 2021;21(18):6065.
- [21] Baccigalupi A, Liccardo A. The huang hilbert transform for evaluating the instantaneous frequency evolution of transient signals in non-linear systems. *Measurement* 2016;86:1–13.
- [22] Chen Z, Mauricio A, Li W, Gryllias K. A deep learning method for bearing fault diagnosis based on cyclic spectral coherence and convolutional neural networks. *Mech Syst Signal Process* 2020;140:106683.
- [23] Ma'D El-Dalahmeh MA-G, Demirel Aykut, Keysan Ozan. Active fault detection using time and frequency diagnostic features for electrical machine. In: The 11th international conference on power electronics, machines and drives; 2022.
- [24] Lavanya S, Prasanth A, Jayachitra S, Shenbagarajan A. A tuned classification approach for efficient heterogeneous fault diagnosis in IOT-enabled WSN applications. *Measurement* 2021;183:109771.
- [25] Liu L, Su J, Liu X, Chen R, Huang K, Deng RH, Wang X. Toward highly secure yet efficient knn classification scheme on outsourced cloud data. *IEEE Internet Things J* 2019;6(6):9841–52.
- [26] Ullah Z, Lodhi BA, Hur J. Detection and identification of demagnetization and bearing faults in PMSM using transfer learning-based VGG. *Energies* 2020;13(15):3834.
- [27] Li Y, Wang Y, Zhang Y, Zhang J. Diagnosis of inter-turn short circuit of permanent magnet synchronous motor based on deep learning and small fault samples. *Neurocomputing* 2021;442:348–58.

Ma'd El-Dalahmeh received a master's degree in Electrical Power and Renewable Energy Resources from Teesside University, U.K., in 2018. Currently, he is pursuing a Ph.D. at Teesside University and working as a research associate on fault detection and identification in electrical machines. His research interests are prognostics, health management of energy storage, signal processing analysis, and artificial intelligence.

Maher Al-Greer received a Ph.D. degree in Electrical Engineering from Newcastle University, Newcastle upon Tyne, U.K., in 2012 and a B.Sc. in Electrical Engineering and M.Sc. in Computer Engineering from the University of Mosul, Iraq, in 1999 and 2005, respectively. He is currently an Associate Professor in Power Conversion and Control at Teesside University, U.K. He has over 15 years' experience in advanced control techniques, power electronics, fault detection and condition monitoring.

Imran Bashir received a Ph.D. in Acoustics from the Open University (2014), U.K., an MSc in Data Communication from the University of Sheffield (2010), and a B.Eng. from COMSATS University (2008). Currently, Imran is a senior lecturer in instrumentations and control at Teesside University. U.K. His research interest includes, acoustic metamaterials, modelling, acoustic characterisation of materials, and condition monitoring.

Mo'ath El-Dalahmeh received an M.Sc. degree in Electrical Power and Renewable Energy Resources from Teesside University, U.K., in 2018. Currently, he is pursuing a Ph.D. at Teesside University. His research activities are concentrated in the fields of prognostics and diagnosis health management for lithium-ion batteries and artificial intelligence.

Aykut Demirel received bachelor's and master's degrees from Middle East Technical University (METU), Ankara, Turkey, in 2015 and 2019, respectively. Currently, he is working at Aselsan. His research interests are condition monitoring and fault diagnosis of electrical motors and motor drives, inverters, gate drivers and power electronics.

Ozan Keysan received a master's degree from Middle East Technical University (METU), Ankara, Turkey, in 2008, and a Ph.D. from the University of Edinburgh, U.K., in 2014. He is currently an associate professor in the Department of Electrical and Electronics Engineering, METU. His current research interests include renewable energy, design and optimisation of electrical machines, smart grids, superconducting machines, and permanent-magnet machines.